5206–5216 *Nucleic Acids Research, 2010, Vol. 38, No. 15* *Published online 12 April 2010*
doi:10.1093/nar/gkq231

Solution structure of the dimerization domain of ribosomal protein P2 provides insights for the structural organization of eukaryotic stalk

Ka-Ming Lee[1,2], Conny Wing-Heng Yu[2], Denise So-Bik Chan[2], Teddy Yu-Hin Chiu[2], Guang Zhu[3], Kong-Hung Sze[4], Pang-Chui Shaw[1,2,*] and Kam-Bo Wong[1,2,*]

[1]Molecular Biotechnology Programme, [2]Department of Biochemistry, Centre for Protein Science and Crystallography, The Chinese University of Hong Kong, [3]Department of Biochemistry, Hong Kong University of Science and Technology and [4]Department of Chemistry, University of Hong Kong, Hong Kong, China

Received February 9, 2010; Revised March 15, 2010; Accepted March 19, 2010

ABSTRACT

The lateral stalk of ribosome is responsible for kingdom-specific binding of translation factors and activation of GTP hydrolysis that drives protein synthesis. In eukaryotes, the stalk is composed of acidic ribosomal proteins P0, P1 and P2 that constitute a pentameric P-complex in 1:2:2 ratio. We have determined the solution structure of the N-terminal dimerization domain of human P2 (NTD-P2), which provides insights into the structural organization of the eukaryotic stalk. Our structure revealed that eukaryotic stalk protein P2 forms a symmetric homodimer in solution, and is structurally distinct from the bacterial counterpart L12 homodimer. The two subunits of NTD-P2 form extensive hydrophobic interactions in the dimeric interface that buries 2400 Å^2 of solvent accessible surface area. We have showed that P1 can dissociate P2 homodimer spontaneously to form a more stable P1/P2 1:1 heterodimer. By homology modelling, we identified three exposed polar residues on helix-3 of P2 are substituted by conserved hydrophobic residues in P1. Confirmed by mutagenesis, we showed that these residues on helix-3 of P1 are not involved in the dimerization of P1/P2, but instead play a vital role in anchoring P1/P2 heterodimer to P0. Based on our results, models of the eukaryotic stalk complex were proposed.

INTRODUCTION

The large subunit of ribosome has a lateral protuberance known as the ribosomal stalk, which is responsible for kingdom-specific binding of translation factors and activation of GTP hydrolysis (1,2). The structural composition of bacterial, archaeal and eukaryotic stalks is different. In bacteria, the stalk consists of ribosomal protein L10 in complex with two or three homodimers of L12 (3,4). In archaeal stalk, L10 is replaced by acidic ribosomal protein P0, which in turn binds three copies of homodimers of P1 (5). The composition of eukaryotic stalk is the most complex, which involves the formation of a pentameric P-complex consisting of acidic ribosomal proteins P0, P1, P2 in 1:2:2 ratio (6). Although early cross-linking experiments suggested the presence of homodimers of P1 and P2 in the eukaryotic P-complex (6), current view favours the model of two copies of P1/P2 heterodimers binding to the C-terminal domain of P0 to form the P0-(P1/P2)2 complex (7,8). The whole P-complex is anchored to the 28S rRNA via the N-terminal domain of P0, which is homologous to the RNA binding domain of L10 (9,10). Eukaryotic P1 and P2 proteins also exist in free form in the cytoplasm, and the exchange between the ribosome-bound and the cytoplasmic pools plays a role in regulating the activity of eukaryotic ribosomes (11).

All P-proteins contain a conserved motif at C-terminus that is responsible for binding elongation factors (12) and ribosome-inactivating proteins (13–15). We have recently solved the crystal structure of the C-terminal conserved motif (SDDDMGFGLFD) of human P-proteins in complex with trichosanthin, a ribosome-inactivating protein, and showed that the two proteins form specific interactions (16). Unlike the flexible C-terminal domain, the N-terminal domains of P1 and P2 form well-ordered helical structures (17), and are involved in the formation of P1/P2 heterodimer (7,18). The P1/P2 heterodimers are anchored to two separate regions in the C-terminal domain of P0 to form the pentameric P-complex (19,20). P2 also exists as a homodimer in the free form (6,21,22), and its N-terminal domain was found to be responsible for

*To whom correspondence should be addressed. Tel: +852 2609 8024; Fax: +852 2603 7246; Email: kbwong@cuhk.edu.hk
Correspondence may also be addressed to Pang-Chui Shaw. Tel: +852 2609 6803; Fax: +852 2603 7246; Email: pcshaw@cuhk.edu.hk

dimerization (7,18,21). Both P1 and P2 are found in the cytoplasmic pool, which are exchanging with those on the ribosome (11). In the absence of P2, P1 is rapidly degraded in yeast (23). Suppression of P2 expression by RNA interference in human cell lines also leads to the depletion of P1 protein (24). These observations suggest that P2 protects P1 from degradation, probably through the formation of P1/P2 heterodimer. To date, high-resolution structure of any eukaryotic P-proteins is not available. To provide better insights into the structural organization of eukaryotic stalk, we have determined the structure of the N-terminal dimerization domain of P2 by nuclear magnetic resonance (NMR) spectroscopy. By homology modelling, a structural model of P1/P2 dimerization domain was proposed and this model correctly predicted that helix-3 of P1 does not involved in P1/P2 dimerization, but plays an important role in the formation of P-complex. Finally, models of the structural organization of eukaryotic stalk were proposed.

MATERIALS AND METHODS

Construction of mutants

The DNA fragments coding for NTD-P1 and NTD-P2 were amplified by PCR using the wild-type expression vectors, pET8c-P1 and pET8c-P2, as templates. NcoI-BamHI digested DNA fragment of NTD-P2 was inserted into pET8c. AgeI-BamHI-digested DNA fragment of NTD-P1 was inserted into an in-house pRSETA-HisSUMO (poly-His-small-ubiquitin-like-modifier) vector, with an N-terminal His-SUMO tag. To create the P1TM mutant, triple mutations (F42D/W43R/L46K) were introduced to the pET8c-P1 using the QuikChange site-directed mutagenesis kit (Stratagene) according to manufacturer instructions. For His-tagged P0, BamHI-EcoRI digested DNA fragment of P0 was inserted into pRSETA vector with an N-terminal poly-histidine tag. Sequences of primers used were summarized in Supplementary Table S1.

Sample preparation

Preparation of NMR samples of NTD-P2. NTD-P2 was expressed in *Escherichia coli* strain BL21(DE3)pLysS (Novagen) in M9 medium (6 g/l Na_2HPO4, 3 g/l KH_2PO4, 0.5 g/l NaCl, 2 mM $MgSO_4$) containing 2 g/l ^{13}C glucose and/or 1 g/l ^{15}N ammonium chloride and appropriate antibiotics (100 μg/ml ampicilin and 50 μg/ml chloramphenicol). To prepare 10% ^{13}C labelled sample, 1.8 g/l ^{12}C glucose plus 0.2 g/l ^{13}C glucose were used instead. Bacterial cells were grown in 37°C until OD_{600} reached 0.4–0.8, when the expression was induced by 0.4 mM isopropyl beta-D-1-thiogalactopyranoside (IPTG). The cells were harvested after 4 h by centrifugation at 6000*g* at 4°C for 10 min.

After sonication, the cell lysate was loaded to a diethylaminoethyl (DEAE)-Sepharose column equilibrated with 20 mM Tris/HCl, pH 8.5. A 200 ml linear gradient of 0–0.3 M NaCl was used to elute NTD-P2. Protein fractions from DEAE-Sepharose column were concentrated to 5 ml before loading to a HiLoad 26/60 Superdex 75 column (GE Healthcare) pre-equilibrated with 20 mM Tris/HCl, 0.2 M NaCl at pH 8.5. Fractions containing the NTD-P2 were pooled, dialysed against 20 mM Tris/HCl at pH 8.5, and then loaded to a 5 ml HiTrap diethylaminopropyl (ANX) column. A gradient of 0–0.2 M NaCl over 200 ml was used to elute the protein and NTD-P2 was eluted at about 0.1 M NaCl. Typical yield for NTD-P2 is 15 mg/l of bacterial culture.

To prepare asymmetrically labelled NTD-P2 for obtaining intermolecular NOEs, 20 μM unlabelled NTD-P2 was mixed with 10 μM $^{13}C/^{15}N$ labelled NTD-P2, denatured in 8 M urea, 0.2 M Na_2SO_4, 20 mM Tris/HCl buffer at pH 7.5, and co-refolded by dialysis against 0.2 M Na_2SO_4, 20 mM Tris/HCl buffer at pH 7.5. Refolded protein complex was concentrated to ~1.7 mM in 0.2 M Na_2SO_4, 20 mM D11-Tris/HCl buffer pH 7.5 in D_2O.

Preparation of NTD-P1/NTD-P2 complex. NTD-P1 was expressed as a fusion protein with an N-terminal His-SUMO tag. His-SUMO-tagged NTD-P1 was expressed as inclusion bodies in *E. coli*, which was washed by 0.1% TritonX-100, 0.1% NP-40, 0.15 M NaCl, 20 mM sodium phosphate buffer (PB) at pH 7.4 and dissolved in 8 M urea, 0.15 M NaCl, 20 mM PB at pH 7.4. After purification by metal-chelating chromatography, 10 μM of urea-denatured His-SUMO-NTD-P1 was mixed with 20 μM NTD-P2, and co-refolded by dialysis against 0.15 M NaCl, 20 mM PB, pH 7.4. Refolded complex of His-SUMO-NTD-P1/NTD-P2 was purified by metal-chelating chromatography. His-SUMO tag was removed by SUMO protease digestion followed by metal-chelating chromatography. NTD-P1/NTD-P2 was further purified by gel filtration using a Superdex 75 column.

Preparation of P1/P2 and P1TM/P2 complex. Cell lysates of P1 or P1TM were loaded to Q fast flow column pre-equilibrated with 20 mM Tris/HCl, pH 7.8. P1 and P1TM collected in flow-through were precipitated by 40% ammonium sulphate. The precipitate was resuspended in 8 M urea, 20 mM Tris/HCl buffer at pH 7.8 and loaded to HiTrap Q HP column pre-equilibrated with the same buffer. P1 or P1TM were eluted by a 200 ml gradient of 0–0.5 M NaCl. After removal of urea by dialysis, P1 or P1TM was mixed with P2 (purified as described previously (13)) in 1:1 molar ratio and was incubated at 4°C for 15 min to yield P1/P2 or P1TM/P2 complex.

Co-refolding of Poly-histidine-tagged P0 with P1/P2 or P1TM/P2

His-tagged P0 was expressed as inclusion bodies in *E. coli*. After expression, the inclusion bodies was washed with 0.1% TritonX-100, 0.1% NP-40 in buffer A (0.5 M NaCl, 20 mM Tris/HCl buffer at pH 7.8), dissolved in 4 M guanidine hydrochloride, and then loaded to a nickel-chelating column pre-equilibrated with 8 M urea in buffer A. His-tagged P0 was eluted by a linear gradient of 0–300 mM imidazole in 8 M urea, buffer A. 10 μM of purified His-tagged P0 was mixed with 30 μM

of purified complex of P1/P2 or P1TM/P2. The proteins were denatured in 8 M urea, and co-refolded by dialysing against buffer A. His-tagged P0 was refolded alone as a control. After co-refolding, the protein samples were centrifuged, and were analysed by sodium dodecyl sulfate polyacrylamide gel electrophoresis (SDS–PAGE). To purify His-tagged P0/P1/P2 complex, the co-refolded protein sample was loaded to a nickel-chelating column pre-equilibrated with buffer A. The complex was eluted by 300 mM imidazole in buffer A.

Structure determination of NTD-P2 by NMR spectroscopy

NMR spectra were collected in a Varian Unity Inova 500 MHz or Bruker Avance 600 MHz spectrometers at 298K. Sequential assignment of backbone resonances was obtained by Cα and Cβ connectivities generated by the HNCACB and the CBCA(CO)NH experiments. Side-chain resonances were obtained from TOCSY-HSQC, HC(CCO)NH, HCCH-TOCSY and HCCH-COSY experiments. Stereo-specific assignment of methyl groups of Val and Leu were based on a constant time ^{1}H-^{13}C HSQC experiment acquired on a 10% ^{13}C-labelled protein sample. The aromatic side-chains of Y3 and Y7 were obtained from 2D homonuclear DQF-COSY and TOCSY experiments. Inter-proton restraints (NOEs) were obtained from NOESY-type experiments such as ^{1}H,^{15}N NOESY-HSQC, ^{1}H,^{15}N HSQC-NOESY-HSQC, ^{1}H,^{13}C-NOESY-HSQC, ^{1}H,^{13}C HSQC-NOESY-HSQC and 2D homonuclear NOESY. Intermolecular NOEs were obtained from the ^{13}C-filtered/^{13}C-edited NOESY (25) acquired on an asymmetrically labelled protein sample of NTD-P2 homodimer. Chemical shifts were referenced with respect to DSS. All multidimensional NMR data were processed with the NMRPipe (26) and analysed using the NMRView software (27). Dihedral angle restraints were derived from the TALOS program (28). Hydrogen bond restraints were deduced from deuterium exchange experiments, and were only included for those protected amide groups in helices. Structural calculation was performed using the program ARIA 2.2 (29) and CNS 1.2 (30,31), with an initial set of manually assigned NOEs. The structures were converged in the first round of calculation. ARIA-assigned NOEs were checked manually, and were included in subsequent rounds of calculation iteratively. Finally, the best 10 structures with the lowest total energy, no NOE or dihedral angle violation were selected. Structural abnormalities in all stages were checked using the program PROCHECK (32).

Static light scattering

100 µl of protein samples (2–4 mg/ml) were loaded to an analytical gel filtration column (Superdex 75 for NTD-P2 homodimer and NTD-P1/NTD-P2; Superdex 200 for P1/P2, P1TM/P2 and P0/P1/P2 complexes) connected to a miniDawn light scattering detector and an Optilab DSP refractometer (Wyatt Technologies). The protein complex was eluted as a single peak. The light scattering data were analysed using the ASTRA software provided by the manufacturer to obtain the molecular mass of the protein complex.

Circular dichroism spectroscopy

Circular dichroism spectra were measured on a JASCO J-810 spectropolarimeter at 298K using a quartz cuvette of 0.1 cm path length. The protein sample concentration was 0.2 mg/ml. The spectra were averages of three scans, and were reported as molar ellipticity.

Urea-induced denaturation

Protein samples (0.2 mg/ml) were equilibrated with 0–7.5 M of urea in 10 mM sodium phosphate buffer at pH 7.4 at 25°C. Protein unfolding was monitored by molar ellipticity at 222 nm at 298K using a 1-mm path-length cuvette with a JASCO J810 spectropolarimeter. The denuatation was confirmed to be reversible. The data were fitted by non-linear regression to a two-state model to obtain the free energy of unfolding (33).

Model building

Models of human P1/P2 dimerization domain and its complex with P0 C-terminal helix were generated by MODELLER (34) using human NTD-P2 and Ph-P0/P1 complex (5) as template respectively. Model of human P-complex built was fit to the extended stalk region of the cryo-EM map of canine 80S ribosome (35) using CHIMERA (36).

RESULTS

P2 forms homodimer and the N-terminal domain is responsible for dimerization

We have constructed the N-terminal domain of human P2 (NTD-P2) by removing 46 residues from the C-terminus. The molecular masses of both full-length P2 and NTD-P2 were analysed by static light scattering and were found to be 22.5 and 13.5 kDa respectively (monomer molecular mass are 11.5 and 7.2 kDa, respectively; Figure 1), suggesting that both of them form homodimer and the N-terminal domain is responsible for dimerization.

NMR structure of NTD-P2

To investigate the structural mechanism of dimerization, we have determined the solution structure of NTD-P2 by NMR spectroscopy. Statistics of structural calculation are summarized in Table 1. NTD-P2 forms a symmetric homodimer, and each monomer has four helices (Figure 2A). The dimeric interface of human NTD-P2 is formed by helices 1, 2 and 4 packing with each other in an antiparallel fashion. Helix-3 is located away from the interface and does not involve in dimerization (Figure 2A). Highly conserved hydrophobic residues Ala-5, Leu-8, Leu-9, Ile-26, Leu-27, Val-30, Ile-32 and Ile-55 are located at the dimeric interface, which buries ~1900 Å^2 of non-polar and ~500 Å^2 of polar solvent accessible surface area (Figure 2B and C). From this point of view, two monomers of NTD-P2 form an integral globular structure consisting of eight helices, with helices 2, 3 and 4

on the surface, and the highly hydrophobic helix-1 buried in the middle of the dimer. In particular, the highly conserved residues (Ala-5, Leu-8 and Leu-9) of helix-1 make a number of interactions in the dimeric interface (Figure 2B). First, Ala-5 and Leu-9 form a ridge that fits into the groove formed by Ala-5 and Leu-8 from the opposite monomer, allowing helix-1 from each monomer to pack according to the ridges-and-grooves model. The Leu-8, on the other hand, is involved in interacting with Ile-55 of helix-4 from the opposite monomer. Moreover, Leu-9 of helix-1 fits nicely into the hydrophobic pocket formed by the conserved residues Ile-26, Val-30 and Ile-32 of helix-2 from the opposite monomer. These interactions are supported by unambiguous intermolecular NOEs observed (Figure 2D).

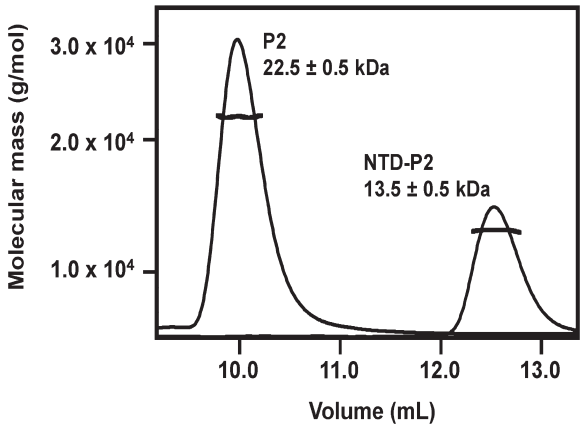

Figure 1. Molecular mass determination of P2 and NTD-P2 by static light scattering. Purified P2 and NTD-P2 were loaded to Superdex 75 (GE healthcare) gel filtration column and analysed by static light scattering. The molecular mass of P2 and NTD-P2 were determined to be 22.5 and 13.5 kDa, respectively (monomer molecular masses are 11.5 and 7.2, respectively), showing that both of them form dimer in solution.

Table 1. NMR and refinement statistics for the 10 best structures of NTD-P2 homodimer

NMR distance and dihedral restraints		
Distance restraints		
Total NOE	2652	
Total unambiguous NOE	2483	
Intramolecular	2345	
Intra-residue	1515	
Sequential (|i–j| = 1)	343	
Medium-range (|i–j| < 5)	257	
Long-range (|i–j| > 4)	230	
Intermolecular	138	
Total ambiguous NOE	169	
Hydrogen bonds	84	
Total dihedral angle restraints		
Φ	78	
Ψ	78	
Structure statistics		
Violations		
Distance restraints[a] (Å)		0.0282 ± 0.0006
Dihedral angle restraint[a] (°)		0.18 ± 0.06
No. of dihedral angle violation >2°		0
No. of distance restraint violation >0.3 Å		0
Deviation from idealized geometry		
Bond lengths[a] (Å)		0.0043 ± 0.0001
Bond angles[a] (°)		0.55 ± 0.01
Impropers[a] (°)		1.75 ± 0.08
Average pairwise r.m.s.d. (Å)		
Heavy		0.80
Backbone		0.33

[a]Values of mean and standard deviation were reported.

P1 and P2 form 1:1 heterodimer spontaneously

We first showed that P1 formed heterodimer with P2 by mixing P1 and P2. The formation of P1/P2 complex was confirmed by native gel electrophoresis (Figure 3A) and size-exclusion-chromatography/static-light-scattering (Figure 3B). The molecular mass of P1/P2 complex was determined to be 24 kDa (Figure 3B), suggesting P1 and P2 form a 1:1 heterodimer in solution (the molecular masses of P1 and P2 are 11.5 and 11.6 kDa, respectively). As P2 alone exists as a homodimer in solution, our data imply that addition of P1 can dissociate P2 homodimer to form a more stable 1:1 P1/P2 heterodimer. To this end, we measured the conformational stability (in terms of free energy of unfolding) of P2 homodimer and P1/P2 heterodimer by urea-induced denaturation experiment. It was found that P1/P2 heterodimer was more stable than P2 homodimer, with free energy of unfolding of 13 kJ/mol and 7 kJ/mol, respectively (Figure 3C). Our result suggests the interaction between P1 and P2 is stronger than that between P2 and P2, which justifies the observation that P1 can dissociate P2 homodimer to form P1/P2 heterodimer spontaneously.

Helix-3 of P1 does not involve in P1/P2 dimerization but is involved in P-complex formation

Previous studies suggested that the N-terminal domains of P1 and P2 are involved in dimerization (18,22,37,38). We have constructed the N-terminal domain of human P1 (NTD-P1) by removing 40 residues from the C-terminus. Purified complex of NTD-P1/NTD-P2 was loaded to Superdex 75 analytical gel filtration column, and the molecular mass of the complex was determined to be 14.8 kDa by static light scattering. Since the molecular masses of NTD-P1 and NTD-P2 are 7.5 and 7.2 kDa, respectively, our data suggest that the N-terminal domain of P1 and P2 also form a 1:1 heterodimer in solution (Figure 3D).

Circular dichroism spectrum of NTD-P1/NTD-P2 heterodimer was similar to that of NTD-P2 homodimer, suggesting that both of them have similar amount of secondary structure content (Supplementary Figure S1A). Moreover, NTD-P1 is predicted to have four helices with pattern similar to NTD-P2 (Supplementary Figure S1B). Taken together, it is very likely that the N-terminal dimerization domains of P1/P2 heterodimer are structurally homologous to NTD-P2. Based on structural homology, we hypothesized that helix-3 of P1 should be located away from the P1/P2 dimerization interface. Noteworthy, the conserved surface charged residues D37, R38 and K41 in helix-3 of P2 are replaced by conserved hydrophobic residues, F42, W43 and L46, in P1 (Figure 4A). It is likely that these residues are

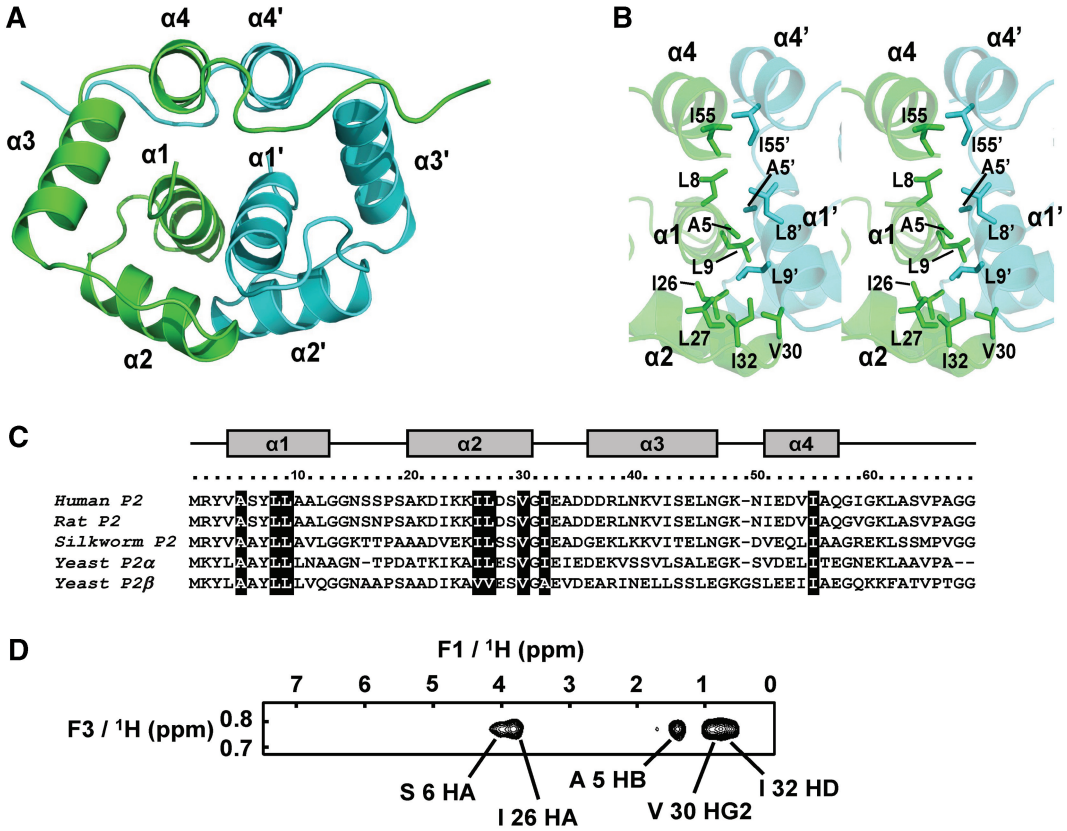

Figure 2. Dimerization mechanism of NTD-P2. (**A**) Topology of helices in symmetric homodimer NTD-P2. NTD-P2 homodimer consists of four helices from each chain. Noteworthy, helix-3 is located away from the dimeric interface formed by helices 1, 2 and 4. (**B**) Stereo-diagram showing the close-up view of the dimeric interface. (**C**) Residues in the dimeric interface are highly conserved (shaded black, A5, L8, L9, I26, L27, V30, I32, I55). Secondary structure elements are indicated above the alignment. (**D**) Intermolecular NOEs were obtained from the three dimensional ^{13}C F_1-filtered, F_3-edited NOESY-HSQC experiment (25) acquired on an asymmetrically labelled NTD-P2 sample. Selected 2D F_1-F_3 plane at ^{13}C frequency (24.2 ppm) of L9 CD2 was shown. L9 HD2 was found to have intermolecular NOE cross peaks to S6 HA, I26 HA, A5 HB, V30 HG2 and I32 HD.

exposed to surface and play a vital role in binding P0. To test this hypothesis, we have created a variant of P1 (P1TM) in which these three hydrophobic residues were substituted to corresponding charged residues in P2 (i.e. F42D/W43R/L46K). To test if the substitutions interfere with P1/P2 heterodimer formation, we mixed full-length human P2 with P1TM. The complexes of P1TM/P2 were purified, and loaded to Superdex 200 analytical gel filtration column. P1TM/P2 eluted as a single symmetrical peak and their molecular masses determined by static light scattering were 22 ± 1 kDa which is in good agreement with the theoretical molecular mass of 23 kDa for 1: 1 binding (Figure 4B). Our results indicate that both P1 (Figure 3B) and P1TM (Figure 4B) were able to form heterodimer with P2 and support the conclusion that helix-3 is not involved in P1/P2 dimerization.

Next, we tested if the substitutions on helix-3 of P1 would affect P-complex formation. Poly-histidine-tagged P0 was co-refolded with purified P1, P2, P1/P2 or P1TM/P2 complex. In the absence of P1 and P2, P0 was aggregated and precipitated after refolding (Figure 4C, lanes 1 and 2). This observation is consistent with previous findings that purification of P0 alone resulted in aggregation (8). If P0 was co-refolded with P1 and P2, a soluble complex containing P0/P1/P2 was detected (Figure 4C, lanes 3 and 4), which was then purified by metal-chelating chromatography. The molecular mass of the complex determined by static light scattering was 80 ± 1 kDa, which is in good agreement with the theoretical molecular mass of 80 kDa for P0-$(P1/P2)_2$ pentameric complex (Figure 4D). If P1 was added, P0 was solubilized with P1 (Figure 4C, lanes 5 and 6). Metal-chelating chromatography showed that P1 was co-eluted with P0, suggesting P0 forms complex with P1. The protein sample was further loaded to a Superdex 200 gel filtration column. The P0/P1 complex was eluted in the void volume, suggesting it forms soluble aggregates. On the other hand, when P0 was co-refolded with P2, P0 was precipitated (Figure 4C, lane 7) while P2 remained soluble in solution (Figure 4C, lane 8), suggesting P2 alone does not form complex with P0. Finally, when P0 was co-refolded with P1TM and P2, P0 was precipitated (Figure 4C, lane 9) while P1TM formed a soluble complex with P2 (Figure 4C, lane 10). This observation strongly suggests that the triple substitutions of the hydrophobic residues on helix-3 of P1 disrupt the interaction of P1/P2 with P0, and failure to co-refold with P1TM and P2 resulted in precipitation of P0. Taken together, our results suggest that helix-3 of P1 is not involved in P1/P2 dimerization but takes part in the formation of P-complex through hydrophobic interaction.

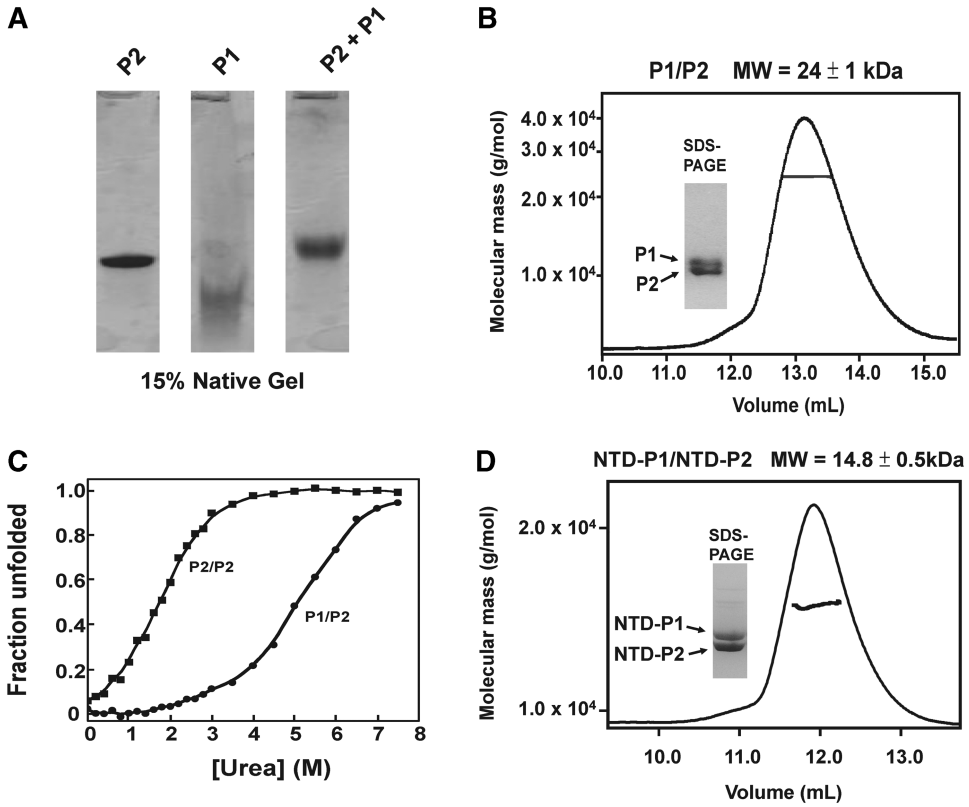

Figure 3. P1 and P2 form 1: 1 heterodimer spontaneously and their N-terminal domain is responsible for dimerization. (**A**) P1/P2 complex was formed by directly mixing P1 and P2. P2 (lane 1) was mixed with P1 (lane 2) in 1: 1 molar ratio. The presence of an up-shifted band in native gel electrophoresis (15% gel in Tris/Glycine buffer at pH 8.8) in lane 3 indicates the formation of P1/P2 complex. (**B**) The protein mixture of P1 and P2 was also loaded to Superdex 200 (GE Healthcare) gel filtration column and analysed by static light scattering. A single peak of P1/P2 complex was eluted, and the eluted protein was analysed by 15% SDS–PAGE (inset). The molecular mass of the P1/P2 complex was determined to be 24 ± 1 kDa (monomer molecular masses of P1 and P2 are 11.5 and 11.6 kDa, respectively), showing that they form 1: 1 heterodimer in solution. (**C**) P1/P2 heterodimer is more stable than P2 homodimer. Conformational stability of P2 homodimer and P1/P2 heterodimer was determined by urea-induced denaturation experiment. Mid-point of transition and *m*-values were 1.7 ± 0.2 M and 3.9 ± 0.4 kJ/mol/M for P2 homodimer, and 4.6 ± 0.3 M, 2.8 ± 0.4 kJ/mol/M for P1/P2 heterodimer. Free energy of unfolding were 7 ± 1 kJ/mol for P2 homodimer and 13 ± 2 kJ/mol for P1/P2 heterodimer. (**D**) N-terminal domain of P1 and P2 forms 1: 1 heterodimer in solution. Purified NTD-P1/NTD-P2 complex was loaded to Superdex 75 column. The molecular mass of the complex estimated by static light scattering was 14.8 ± 0.5 kDa, suggesting the formation of 1: 1 heterodimer. The inset shows SDS–PAGE analysis of purified NTD-P1/NTD-P2 complex. The theoretical molecular masses of monomeric NTD-P1 and NTD-P2 are 7.5 and 7.2 kDa, respectively.

DISCUSSION

Although the ribosomal stalks are present in ribosomes from all three domains of life, their structural compositions are different. In bacteria, the stalk complex is constituted by 2–3 copies of L12 dimer binding to L10 via a C-terminal spine helix (3,4,39). In archaeal stalk, three copies of P1 homodimers bind to P0 via three helices of the C-terminal spine (5). Although there was no high resolution structure of any eukaryotic stalk protein, it is generally believed that two copies of P1/P2 heterodimers bind to the C-terminal of P0 to form a pentameric P-complex (12). The structure of the dimerization domain of human ribosomal protein reported in this study provides insights into the organization of eukaryotic stalk.

Structural comparison of the dimerization domains of eukaryotic, bacterial and archaeal stalk proteins

As expected from the large sequence divergence between eukaryotic and bacterial stalk proteins, the structure of NTD-P2 is very different from that of the bacterial L12 dimer. The 30-residues N-terminal domain of L12 consists of two helices forming a V-shaped hairpin and two antiparallel V-shaped α–α hairpins entangled with each other to form the hydrophobic dimeric interface (4,40,41) (Figure 5). In contrast, the N-terminal dimerization domain of P2 (NTD-P2) has about 70 residues and the dimeric interface is formed by helices 1, 2 and 4 packing with each other in an antiparallel fashion with helix-3 locating away from the interface.

On the other hand, human NTD-P2 shares structural and sequence similarity with archaeal P1 protein. The recent crystal structure of archaeal $P0(P1)_2(P1)_2(P1)_2$ stalk complex from *Pyrococcus horikoshii* showed that each of the P1 (Ph-P1) homodimer binds to C-terminal spine helix of P0 (Ph-P0) (5). The sequence identity between the dimerization domains of human P2 and Ph-P1 is 29%. Similar to NTD-P2, each monomer of Ph-P1 has four helices. Helix-1 and 2 of the Ph-P1 lay at the dimerization interface in an antiparallel fashion while helix-3 is packed away from the interface. The major

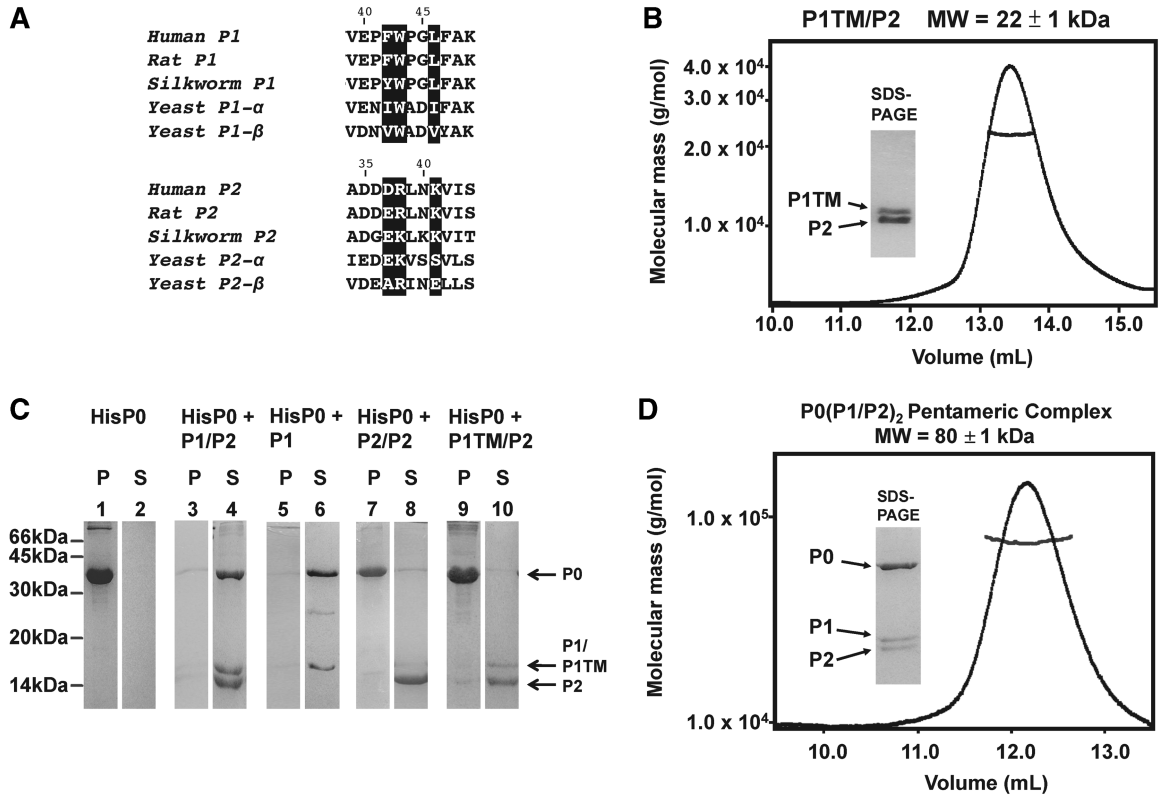

Figure 4. Conserved hydrophobic residues on helix-3 of P1 is responsible for P0 binding but not for P1/P2 dimerization. (**A**) Three conserved charged residues (D37, R38 and K41) on helix-3 of human P2 were found to be substituted by conserved hydrophobic residues (F42, W43 and L46) in P1. A triple substituted variant of P1 (P1TM, F42D/W43R/L46K) was constructed to test the role of these residues in P-complex formation. (**B**) P1TM can interact with P2 to form 1: 1 heterodimer. P1TM was mixed with P2 in 1: 1 molar ratio, and was then loaded to Superdex 200 (GE Healthcare) gel filtration column and analysed by static light scattering. A single peak of P1TM/P2 complex was eluted, and the eluted protein was analysed by 15% SDS–PAGE (inset). The molecular mass of P1TM/P2, estimated by static light scattering, suggests the formation of 1: 1 heterodimer. (**C**) Conserved residues on helix-3 of P1 are involved in binding P0. Poly-histidine-tagged P0 (HisP0) was refolded alone (lanes 1 and 2), with P1/P2 (lanes 3 and 4), with P1 (lanes 5 and 6), with P2/P2 (lanes 7 and 8) or with P1TM/P2 (lanes 9 and 10). After refolding, the protein samples were centrifuged. The pellet (lanes 1, 3, 5, 7 and 9) and the soluble fractions (lanes 2, 4, 6, 8 and 10) were analysed by 15% SDS–PAGE. (**D**) P0, P1 and P2 form pentameric P-complex in 1: 2: 2 ratio. The refolded complex of P0/P1/P2 (Figure 4C, lane 4) was first purified by metal-chelating chromatography and then loaded to Superdex 200 (GE Healthcare) gel filtration column and analysed by static light scattering. The molecular mass of the P-complex was determined to be 80 kDa, which is consistent with the stoichiometry of P0:P1:P2 = 1: 2: 2 for HisP0, P1 and P2 having molecular masses of 34, 11.5 and 11.6 kDa, respectively.

structural differences are found on helix-4. In human P2, helix-4 adopts a closed conformation in which it packs on helix-1 and 3 forming an intact hydrophobic core. In contrast, helix-4 of Ph-P1 adopts an open conformation that exposes a hydrophobic pocket for binding of Ph-P0 (Figure 5). It is likely that the structure of free Ph-P1 homodimer resembles the structure of human NTD-P2 reported here, and a 'lid-opening' motion of helix-4 is required for Ph-P1 to bind Ph-P0.

Insights into structural organization of eukaryotic stalk complex

In contrast to archaeal stalk complex, eukaryotic P0 binds heterodimers of P1/P2 instead of homodimers of P1 or P2 (7,8). Consistent with previous studies, here we show that while eukaryotic P2 alone forms homodimer in solution, it forms P1/P2 heterodimer spontaneously in the presence of P1 (Figure 3) (8,21,22,42,43). We have showed that the stability (as measured by free energy of unfolding) of human P1/P2 heterodimer is higher than that of P2 homodimer. Our results are consistent with previous findings that P1/P2 retains a higher proportion of dimeric form than P2 homodimer in mass spectrometry spectra (22). The fact that P1/P2 heterodimer is more stable than P2 homodimer suggests that P2 forms stronger interaction with P1. This allows P1 to dissociate P2 homodimer spontaneously to form P1/P2 heterodimer, which then binds to P0.

Homology modelling of P1/P2 heterodimer predicts that three exposed polar residues on helix-3 of P2 are replaced by conserved hydrophobic residues in P1. As a result, P1/P2 heterodimer is asymmetrical in the sense that the surface of helix-3 on the P1 side is hydrophobic, while that on the P2 side is hydrophilic (Supplementary Figure S1B and C). Based on this model, we correctly predicted that these conserved hydrophobic residues are not involved in the formation of P1/P2 heterodimer, but play an important role in anchoring P1/P2 heterodimer to P0 (Figure 4). Replacing these hydrophobic residues with hydrophilic ones disrupted the formation of eukaryotic stalk complex.

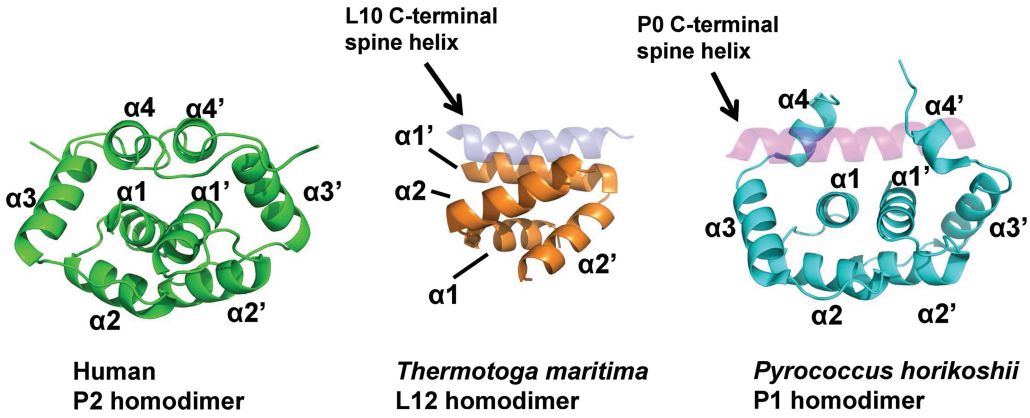

Figure 5. Structural comparison among eukaryotic, bacterial and archaeal stalk proteins. The structure of human P2 homodimer (green) is compared with the structure of bacterial (*Thermotoga maritima*, orange) L12 homodimer (4,40,41) and of archaeal (*Pyrococcus horikoshii*, cyan) P1 homodimer (5). The C-terminal spine helices of bacteria L10 and archaeal P0 are in purple and magenta, respectively.

How do these conserved residues on helix-3 of P1 contribute to the formation of P-complex? In the crystal structure of the archaeal stalk complex, Ph-P0 binds to three copies of Ph-P1 homodimers, and the helix-3 of P1 makes contacts with helix-3 of adjacent Ph-P1 homodimers (5) (Supplementary Figure S2A). In contrast, eukaryotic P0 binds two copies of P1/P2 heterodimers. The asymmetry of P1/P2 heterodimer results in four possibilities of topological arrangements: (i) P1/P2:P1/P2; (ii) P1/P2:P2/P1; (iii) P2/P1:P2/P1; (iv) P2/P1:P1/P2 (Supplementary Figure S2B). All of these arrangements are consistent with the findings that P0 can be cross-linked to both P1 and P2 (6). If the eukaryotic stalk complex has similar structural organization to archaeal stalk complex, our results favour the topological arrangement of P2/P1:P1/P2 (Figure 6A), in which two helix-3 from adjacent P1 are facing each other. Homology modelling of the P-complex suggested that the conserved hydrophobic residues (Phe42, Trp43, Leu46) on helix-3 of P1 can form hydrophobic interactions with adjacent P1 and with a conserved Tyr-Pro motif of P0 at the loop between the two spine helices (Supplementary Figure S3A–C). This model is consistent with the observation that Trp43 in helix-3 of P1 is buried in the yeast pentameric P-complex (44). Substituting these conserved residues with hydrophilic one from P2 will break the hydrophobic interactions between P0 and P1, and introduce charge–charge repulsion between adjacent P1 (Supplementary Figure S3B), leading to the disruption of eukaryotic stalk complex (Figure 4). This model also predicts that the binding of two P1/P2 heterodimers are cooperative, which is consistent with previous finding that removal of one of the two P1/P2 binding sites from P0 weaken its interaction with P1/P2 (19).

In the cryo-EM map of canine 80S ribosome (35), there is an un-interpreted density at the extended stalk region (Figure 6B). Initial inspection suggested that the density is big enough to accommodate two copies of P1/P2 heterodimers. A model of the dimerization domains of P-complex, with topological arrangement of P2/P1:P1/P2, was generated by homology modelling (Supplementary Figure S3A). This model can be nicely fitted into the cryo-EM density at the extended stalk region (Figure 6B). Similarly, the model can also be fitted to the cryo-EM map of yeast 80S ribosome in complex with elongation factor 2 (45) (Supplementary Figure S4). There is a conserved motif SDDDMGFGLFD at the C-termini of eukaryotic P-proteins, which is involved in functional binding of elongation factors (12) and ribosomal inactivating proteins (13). In the crystal structure of the C-terminal motif in complex with a ribosomal inactivating protein, trichosanthin, the GFGLF motif adopts a type-II β-turn conformation that docks the Leu-Phe residues into a small hydrophobic pocket of trichosanthin (16). The C-terminal conserved motif is linked to the dimerization domain of P-proteins via a flexible linker. As showed in Figure 6B, the flexible C-terminal tails of P-proteins are protruding out of the extended stalk and are in positions for making interactions with bound translation factors and recruiting translation factors to the ribosome (12,46).

Despite the differences in sequence and structural composition, stalk complexes from bacteria, archaea and eukaryotes share similar functional organization (Supplementary Figure S5). They all have a 'scaffold' protein (L10 in bacteria and P0 in archaea and eukaryotes) that has an N-terminal domain for anchoring to the rRNA, and a spine helix that binds dimers of small ribosomal stalk proteins (L12 in bacteria, P1 in archaea and P1/P2 in eukaryotes). In these small ribosomal stalk proteins, the N-terminal dimerization domain responsible for interacting with the scaffold proteins (L10 or P0) is connecting via a flexible linker to the C-terminal domain responsible for binding translation factors (4,5,12,47). As a result, stalk complexes from all three kingdoms have multiple copies of the C-terminal domain protruding out from the ribosomal stalk. This similarity in functional organization is likely to reflect a common mechanism in translation factor recruitment. For example, it has been suggested that multiple copies of the C-terminal domain increase the probability of encountering translation factors in the cytoplasm, and fetch them to the factor binding site (4,5).

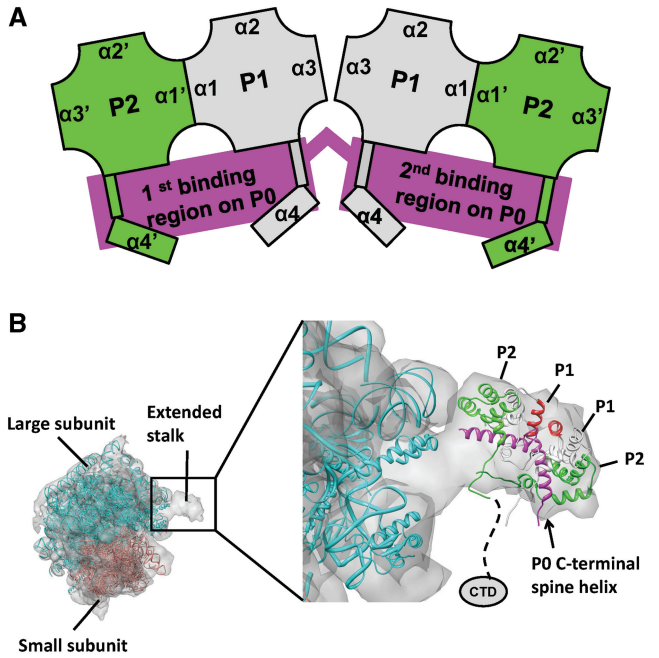

Figure 6. Structural organization of eukaryotic stalk complex. (**A**) Proposed topological arrangement of eukaryotic stalk complex. The two P1/P2 heterodimers are arranged in such a way that their helix-3 of P1 are facing each other. This arrangement is consistent with our results that the conserved residues on helix-3 of P1 are vital to the formation of the eukaryotic stalk complex. (**B**) The structural model of the dimerization domain of eukaryotic stalk complex was fitted into the cryo-EM map of the canine 80S ribosome (35) by CHIMERA (36). P0, helix-3 of P1 and P2 are colour coded in magenta, red and green, respectively. The C-terminal domain (CTD) of P-proteins, which is extending out from the dimerization domain of the P-complex via a flexible linker (dotted line), should be in vicinity to make interactions with translation factors.

It has been observed that while P0 can be solubilized by P1, it cannot form a soluble complex with the addition of P2 alone (7,42). Our co-refolding experiments came to the same conclusion (Figure 4C). Based on this observation, another model for eukaryotic stalk complex was proposed previously (7). In this model, P1 is located between P0 and P2, and serves as a bridge between them in the eukaryotic stalk complex (Supplementary Figure S6). If this topological arrangement is correct, the conserved hydrophobic residues on helix-3 of eukaryotic P1 may be involved in direct interaction with P0. Alternatively, the same observation can be explained by our model of P-complex (Supplementary Figure S3). Similar to P1TM, the formation of P0/P2 complex may be prevented by the hydrophilic residues on helix-3 of P2. In the case of the P0/P1 complex, it formed soluble aggregates in our hand. If the P0/P1 complex is structurally homologous to the archaeal stalk complex, the exposed conserved hydrophobic residues on helix-3 of P1 may lead to the observed aggregation of P0/P1 complex (Supplementary Figure S3D). Structure determination of eukaryotic P-complex, which is underway in our laboratory, will provide a definite answer to the structural organization of eukaryotic stalk.

ACCESSION NUMBER

Atomic coordinates for the refined structures have been deposited with the Protein Data Bank under accession code 2W1O.

SUPPLEMENTARY DATA

Supplementary Data are available at NAR Online.

ACKNOWLEDGEMENTS

Molecular graphics images in Figure 6 and Supplementary Figure S4 were produced using the UCSF Chimera package from the Resource for Biocomputing, Visualization and Informatics at the University of California, San Francisco (supported by NIH P41 RR-01081). Other molecular images were produced by PyMOL.

FUNDING

General Research Fund (Project no. 430103 and 477509) from the Research Grants Council of Hong Kong SAR. The funders had no role in study design, data collection and analysis, decision to publish or preparation of the manuscript. Funding for open access charge: The Chinese University of Hong Kong.

Conflict of interest statement. None declared.

REFERENCES

1. Uchiumi,T., Honma,S., Nomura,T., Dabbs,E.R. and Hachimori,A. (2002) Translation elongation by a hybrid ribosome in which proteins at the GTPase center of the Escherichia coli ribosome are replaced with rat counterparts. *J. Biol. Chem.*, **277**, 3857–3862.
2. Uchiumi,T., Hori,K., Nomura,T. and Hachimori,A. (1999) Replacement of L7/L12.L10 protein complex in Escherichia coli ribosomes with the eukaryotic counterpart changes the specificity of elongation factor binding. *J. Biol. Chem.*, **274**, 27578–27582.
3. Pettersson,I., Hardy,S.J. and Liljas,A. (1976) The ribosomal protein L8 is a complex L7/L12 and L10. *FEBS Lett.*, **64**, 135–138.
4. Diaconu,M., Kothe,U., Schlunzen,F., Fischer,N., Harms,J.M., Tonevitsky,A.G., Stark,H., Rodnina,M.V. and Wahl,M.C. (2005) Structural basis for the function of the ribosomal L7/12 stalk in factor binding and GTPase activation. *Cell*, **121**, 991–1004.
5. Naganuma,T., Nomura,N., Yao,M., Mochizuki,M., Uchiumi,T. and Tanaka,I. (2010) Structural basis for translation factor recruitment to the eukaryotic/archaeal ribosomes. *J. Biol. Chem.*, **285**, 4747–4756.
6. Uchiumi,T., Wahba,A.J. and Traut,R.R. (1987) Topography and stoichiometry of acidic proteins in large ribosomal subunits from Artemia salina as determined by crosslinking. *Proc. Natl Acad. Sci. USA*, **84**, 5580–5584.
7. Gonzalo,P., Lavergne,J.P. and Reboud,J.P. (2001) Pivotal role of the P1 N-terminal domain in the assembly of the mammalian

ribosomal stalk and in the proteosynthetic activity. *J. Biol. Chem.*, **276**, 19762–19769.
8. Shimizu,T., Nakagaki,M., Nishi,Y., Kobayashi,Y., Hachimori,A. and Uchiumi,T. (2002) Interaction among silkworm ribosomal proteins P1, P2 and P0 required for functional protein binding to the GTPase-associated domain of 28S rRNA. *Nucleic Acids Res.*, **30**, 2620–2627.
9. Santos,C. and Ballesta,J.P. (2005) Characterization of the 26S rRNA-binding domain in Saccharomyces cerevisiae ribosomal stalk phosphoprotein P0. *Mol. Microbiol.*, **58**, 217–226.
10. Musters,W., Concalves,P.M., Boon,K., Raue,H.A., van Heerikhuizen,H. and Planta,R.J. (1991) The conserved GTPase center and variable region V9 from Saccharomyces cerevisiae 26S rRNA can be replaced by their equivalents from other prokaryotes or eukaryotes without detectable loss of ribosomal function. *Proc. Natl Acad. Sci. USA*, **88**, 1469–1473.
11. Ballesta,J.P. and Remacha,M. (1996) The large ribosomal subunit stalk as a regulatory element of the eukaryotic translational machinery. *Prog. Nucleic Acid Res. Mol. Biol.*, **55**, 157–193.
12. Gonzalo,P. and Reboud,J.P. (2003) The puzzling lateral flexible stalk of the ribosome. *Biol. Cell*, **95**, 179–193.
13. Chan,D.S., Chu,L.O., Lee,K.M., Too,P.H., Ma,K.W., Sze,K.H., Zhu,G., Shaw,P.C. and Wong,K.B. (2007) Interaction between trichosanthin, a ribosome-inactivating protein, and the ribosomal stalk protein P2 by chemical shift perturbation and mutagenesis analyses. *Nucleic Acids Res.*, **35**, 1660–1672.
14. McCluskey,A.J., Poon,G.M., Bolewska-Pedyczak,E., Srikumar,T., Jeram,S.M., Raught,B. and Gariepy,J. (2008) The catalytic subunit of shiga-like toxin 1 interacts with ribosomal stalk proteins and is inhibited by their conserved C-terminal domain. *J. Mol. Biol.*, **378**, 375–386.
15. Chiou,J.C., Li,X.P., Remacha,M., Ballesta,J.P. and Tumer,N.E. (2008) The ribosomal stalk is required for ribosome binding, depurination of the rRNA and cytotoxicity of ricin A chain in Saccharomyces cerevisiae. *Mol. Microbiol.*, **70**, 1441–1452.
16. Too,P.H., Ma,M.K., Mak,A.N., Wong,Y.T., Tung,C.K., Zhu,G., Au,S.W., Wong,K.B. and Shaw,P.C. (2009) The C-terminal fragment of the ribosomal P protein complexed to trichosanthin reveals the interaction between the ribosome-inactivating protein and the ribosome. *Nucleic Acids Res.*, **37**, 602–610.
17. Tchorzewski,M., Krokowski,D., Boguszewska,A., Liljas,A. and Grankowski,N. (2003) Structural characterization of yeast acidic ribosomal P proteins forming the P1A-P2B heterocomplex. *Biochemistry*, **42**, 3399–3408.
18. Naganuma,T., Shiogama,K. and Uchiumi,T. (2007) The N-terminal regions of eukaryotic acidic phosphoproteins P1 and P2 are crucial for heterodimerization and assembly into the ribosomal GTPase-associated center. *Genes Cells*, **12**, 501–510.
19. Hagiya,A., Naganuma,T., Maki,Y., Ohta,J., Tohkairin,Y., Shimizu,T., Nomura,T., Hachimori,A. and Uchiumi,T. (2005) A mode of assembly of P0, P1, and P2 proteins at the GTPase-associated center in animal ribosome: in vitro analyses with P0 truncation mutants. *J. Biol. Chem.*, **280**, 39193–39199.
20. Krokowski,D., Boguszewska,A., Abramczyk,D., Liljas,A., Tchorzewski,M. and Grankowski,N. (2006) Yeast ribosomal P0 protein has two separate binding sites for P1/P2 proteins. *Mol. Microbiol.*, **60**, 386–400.
21. Tchorzewski,M., Boguszewska,A., Dukowski,P. and Grankowski,N. (2000) Oligomerization properties of the acidic ribosomal P-proteins from Saccharomyces cerevisiae: effect of P1A protein phosphorylation on the formation of the P1A-P2B hetero-complex. *Biochim. Biophys. Acta*, **1499**, 63–73.
22. Grela,P., Sawa-Makarska,J., Gordiyenko,Y., Robinson,C.V., Grankowski,N. and Tchorzewski,M. (2008) Structural properties of the human acidic ribosomal P proteins forming the P1-P2 heterocomplex. *J. Biochem.*, **143**, 169–177.
23. Nusspaumer,G., Remacha,M. and Ballesta,J.P. (2000) Phosphorylation and N-terminal region of yeast ribosomal protein P1 mediate its degradation, which is prevented by protein P2. *EMBO J.*, **19**, 6075–6084.
24. Martinez-Azorin,F., Remacha,M. and Ballesta,J.P. (2008) Functional characterization of ribosomal P1/P2 proteins in human cells. *Biochem J.*, **413**, 527–534.
25. Zwahlen,C., Legault,P., Vincent,S.J.F., Greenblatt,J., Konrat,R. and Kay,L.E. (1997) Methods for measurement of intermolecular NOEs by multinuclear NMR spectroscopy: application to a bacteriophage lambda N-peptide/boxB RNA complex. *J. Am. Chem. Soc.*, **119**, 6711–6721.
26. Delaglio,F., Grzesiek,S., Vuister,G.W., Zhu,G., Pfeifer,J. and Bax,A. (1995) NMRPipe: a multidimensional spectral processing system based on UNIX pipes. *J. Biomol. NMR*, **6**, 277–293.
27. Johnson,B.A. and Blevins,R.A. (1994) NMRView: a computer program for the visualization and analysis of NMR data. *J. Biomol. NMR*, **4**, 603–614.
28. Cornilescu,G., Delaglio,F. and Bax,A. (1999) Protein backbone angle restraints from searching a database for chemical shift and sequence homology. *J. Biomol. NMR*, **13**, 289–302.
29. Linge,J.P., O'Donoghue,S.I. and Nilges,M. (2001) Automated assignment of ambiguous nuclear overhauser effects with ARIA. *Methods Enzymol.*, **339**, 71–90.
30. Brunger,A.T., Adams,P.D., Clore,G.M., DeLano,W.L., Gros,P., Grosse-Kunstleve,R.W., Jiang,J.S., Kuszewski,J., Nilges,M., Pannu,N.S. *et al.* (1998) Crystallography & NMR system: a new software suite for macromolecular structure determination. *Acta Cryst.*, **D54**, 905–921.
31. Brunger,A.T. (2007) Version 1.2 of the crystallography and NMR system. *Nat. Protoc.*, **2**, 2728–2733.
32. Laskowski,R.A., Rullmannn,J.A., MacArthur,M.W., Kaptein,R. and Thornton,J.M. (1996) AQUA and PROCHECK-NMR: programs for checking the quality of protein structures solved by NMR. *J. Biomol. NMR*, **8**, 477–486.
33. Santoro,M.M. and Bolen,D.W. (1988) Unfolding free energy changes determined by the linear extrapolation method. 1. Unfolding of phenylmethanesulfonyl alpha-chymotrypsin using different denaturants. *Biochemistry*, **27**, 8063–8068.
34. Marti-Renom,M.A., Stuart,A.C., Fiser,A., Sanchez,R., Melo,F. and Sali,A. (2000) Comparative protein structure modeling of genes and genomes. *Annu. Rev. Biophys. Biomol. Struct.*, **29**, 291–325.
35. Chandramouli,P., Topf,M., Ménétret,J.F., Eswar,N., Cannone,J.J., Gutell,R.R., Sali,A. and Akey,C.W. (2008) Structure of the mammalian 80S ribosome at 8.7 A resolution. *Structure*, **16**, 535–548.
36. Pettersen,E.F., Goddard,T.D., Huang,C.C., Couch,G.S., Greenblatt,D.M., Meng,E.C. and Ferrin,T.E. (2004) UCSF Chimera–a visualization system for exploratory research and analysis. *J. Comput. Chem.*, **25**, 1605–1612.
37. Briceno,V., Camargo,H., Remacha,M., Santos,C. and Ballesta,J.P. (2009) Structural and functional characterization of the amino terminal domain of the yeast ribosomal stalk P1 and P2 proteins. *Int. J. Biochem. Cell Biol.*, **41**, 1315–1322.
38. Grela,P., Helgstrand,M., Krokowski,D., Boguszewska,A., Svergun,D., Liljas,A., Bernado,P., Grankowski,N., Akke,M. and Tchorzewski,M. (2007) Structural characterization of the ribosomal P1A-P2B protein dimer by small-angle X-ray scattering and NMR spectroscopy. *Biochemistry*, **46**, 1988–1998.
39. Gudkov,A.T., Tumanova,L.G., Venyaminov,S.Y. and Khechinashvilli,N.N. (1978) Stoichiometry and properties of the complex between ribosomal proteins L7 and L10 in solution. *FEBS Lett.*, **93**, 215–218.
40. Wahl,M.C., Bourenkov,G.P., Bartunik,H.D. and Huber,R. (2000) Flexibility, conformational diversity and two dimerization modes in complexes of ribosomal protein L12. *EMBO J.*, **19**, 174–186.
41. Bocharov,E.V., Sobol,A.G., Pavlov,K.V., Korzhnev,D.M., Jaravine,V.A., Gudkov,A.T. and Arseniev,A.S. (2004) From structure and dynamics of protein L7/L12 to molecular switching in ribosome. *J. Biol. Chem.*, **279**, 17697–17706.
42. Zurdo,J., Parada,P., van den Berg,A., Nusspaumer,G., Jimenez-Diaz,A., Remacha,M. and Ballesta,J.P. (2000) Assembly of Saccharomyces cerevisiae ribosomal stalk: binding of P1 proteins is required for the interaction of P2 proteins. *Biochemistry*, **39**, 8929–8934.

43. Tchorzewski,M., Boldyreff,B., Issinger,O. and Grankowski,N. (2000) Analysis of the protein-protein interactions between the human acidic ribosomal P-proteins: evaluation by the two hybrid system. *Int. J. Biochem. Cell Biol.*, **32**, 737–746.
44. Grela,P., Krokowski,D., Gordiyenko,Y., Krowarsch,D., Robinson,C.V., Otlewski,J., Grankowski,N. and Tchorzewski,M. (2010) Biophysical properties of the eukaryotic ribosomal stalk. *Biochemistry*, **49**, 924–933.
45. Spahn,C.M., Gomez-Lorenzo,M.G., Grassucci,R.A., Jorgensen,R., Andersen,G.R., Beckmann,R., Penczek,P.A., Ballesta,J.P. and Frank,J. (2004) Domain movements of elongation factor eEF2 and the eukaryotic 80S ribosome facilitate tRNA translocation. *EMBO J.*, **23**, 1008–1019.
46. Gomez-Lorenzo,M.G., Spahn,C.M., Agrawal,R.K., Grassucci,R.A., Penczek,P., Chakraburtty,K., Ballesta,J.P., Lavandera,J.L., Garcia-Bustos,J.F. and Frank,J. (2000) Three-dimensional cryo-electron microscopy localization of EF2 in the Saccharomyces cerevisiae 80S ribosome at 17.5 A resolution. *EMBO J.*, **19**, 2710–2718.
47. Wahl,M.C. and Moller,W. (2002) Structure and function of the acidic ribosomal stalk proteins. *Curr. Protein Pept. Sci.*, **3**, 93–106.